Vibration Reduction In Rotorcraft Using Actively Controlled Flaps - Their Evolution and Potential for Improving Rotorcraft Technology

Peretz P. Friedmann
François-Xavier Bagnoud Professor of Aerospace Engineering
peretzf@umich.edu
Department of Aerospace Engineering
University of Michigan, Ann Arbor, Michigan 48109-2140

Abstract

This paper describes research on actively controlled partial span trailing edge flaps used for vibration reduction in rotorcraft. It traces the evolution of this concept and describes the basic features of aeroelastic simulation codes needed for predicting the performance of actively controlled flaps. Validation of a simulation code is also presented by comparing the results obtained with experimental data. The vibration reduction potential of this effective vibration control approach is illustrated by several examples. Full scale implementations of this approach being pursued in both the US and Europe are also discussed. Recent research has also demonstrated that the actively controlled flap has considerable potential for noise reduction. Simultaneous noise and vibration reduction has been also shown in simulation. Therefore actively controlled flaps have a remarkable potential for improving rotorcraft technology.

Introduction and Objectives

One of the primary concerns in rotorcraft design is the issue of vibrations experienced in the fuselage and its reduction. High levels of vibration may lead to passenger discomfort, fatigue of helicopter components, reduced effectiveness of weapon systems and increased noise and cost. The largest contributor to vibrations in a helicopter is the rotor. Initially, passive control approaches consisting of vibration absorbers and isolators were used for vibration reduction. However, stringent requirements for low vibration levels (less than 0.05g) imposed during the last 25 years have led to the development of active approaches to vibration reduction.

A careful comparison of some of the approaches developed for vibration control, in pursuit of the objective of achieving a "jet smooth" ride in rotary wing vehicles is presented in Ref. [1]. During the last 25 years, three basic approaches to active vibration control in rotorcraft have emerged [1]. The first approach developed was higher harmonic control (HHC). In this approach, pitch inputs are introduced through the conventional swashplate in the hub fixed system. All blades experience the same input, and the vibratory aerodynamic loads are modified at their source, in the rotor, before they propagate into the fuselage. Details on this approach can be found in Refs. [1] and [2]. The first operational HHC system was flight tested on an OH-6A helicopter in 1983-84 [3], and very good vibration reduction was demonstrated in the closed loop mode up to airspeeds of 100 knots. Flight tests of an experimental HHC system on a SA349 Gazelle were also conducted in France in 1985 [4] using the same HHC control algorithm [1–3] and a reduction of 80% in cabin vibrations was demonstrated at an airspeed of 250 kmph. It is important to note that despite the demonstrated feasibility of the HHC approach and its relative maturity, this technology has not been implemented on an actual production helicopter. There are several reasons for this situation: (1) limitation of the approach due to the requirement to provide the same pitch input to all the blades, (2) the high cost of implementing the approach on a production helicopter, due to the fact that pitch angles are introduced through the primary control system, i.e. the swashplate, and (3) higher power requirements when using this approach on hingeless or bearingless rotors [5].

A more promising alternative is individual blade control (IBC), where time varying pitch is introduced directly into the rotating frame, and different control inputs can be provided to each blade [1]. The IBC ap-

Presented at the 30th European Rotorcraft Forum, Marseille, France, September 14-16, 2004. *Copyright ©2004 by the author. All rights reserved.*

proach can be implemented using three different techniques:

(a) One can oscillate the entire blade in pitch by actuating it at the root; this approach was used in the earliest implementation of the IBC methodology [1]. For convenience, this implementation will be denoted as classical IBC (CIBC) approach.

(b) Alternatively, one or more partial span trailing edge flaps, shown in Fig. 1, can be actuated on the blade, this approach is often called the actively controlled flap (ACF) [1, 6]. The ACF approach can be implemented in single or dual flap configurations. Since each flap can be individually controlled in the rotating system, this is simply another version of the IBC approach.

(c) A third implementation twists the entire blade by embedding piezoelectric fibers, this approach is known as the Active Twist Rotor (ATR). The blade structure for this configuration, shown schematically in Fig. 2, was developed jointly by MIT, the Army and NASA Langley Research Center [7, 8].

All three implementations of the IBC approach have proven themselves to be quite effective in reducing vibrations. However, the level of maturity for each differs and the potential for practical implementation on a production helicopter is also quite different. The conventional IBC approach is quite mature. It has been tested on a full scale MBB BO-105 rotor both in the wind tunnel [9] as well as in flight [10]. The primary difficulty with this approach is the mechanical complexity of the system [9, 10] and the fact that its best implementation may require the replacement of the conventional swashplate by an "electronic" counterpart. Again, these two factors combine to increase the cost of the system beyond a level that is considered to be currently economically viable.

The ACF has been studied extensively, using aeroelastic simulations, and it has been tested on scaled rotors in the wind tunnel. A full-scale wind tunnel test of the system is imminent, as will be shown later in the paper. The primary advantage of the ACF compared to the other approaches is due to several factors [1]: (1) significantly lower power consumption for actuation than either CIBC or ATR, (2) relative simplicity of implementation, and (3) airworthiness issues, since the flaps are independent of the primary control system (i.e. the swashplate), their malfunction will not affect the helicopter's airworthiness.

The ATR implementation is the least mature. It has been simulated and tested in the wind tunnel on a scaled rotor. However, the full-scale implementation of this approach on a particular rotor system is not currently under consideration.

Finally, it is important to note that in addition to the demonstrated capability of the IBC approach to reduce vibratory loads, it also has considerable potential for noise reduction and performance enhancement. All the active control approaches described above control vibrations in the rotating frame, i.e. the rotor, and attempt to reduce the vibration at their source before they propagate into the fuselage.

A third, alternative, approach to vibration control known as active control of structural response (ACSR) is aimed at controlling vibrations in the fuselage or the fixed frame as illustrated in Fig. 3. In this approach, stiff actuators introduce small amplitude excitation between the rotor and the fuselage, such that the sum of the response of the airframe at specified locations, due to rotor loads and the excitation due to controls, is reduced to a minimum. It is important to note that among various active approaches, only the ACSR system has been actually installed on a production helicopter, the EH101, built by an European partnership between Westland and Augusta [11, 12].

From this literature review, it is evident that among the various active control approaches, IBC implemented using the single or dual flap configuration appears to be the most promising concept. Its characteristics, methods of actuation and implementation on actual full-scale rotorcraft have been and are currently studied. The remarkable potential of the ACF for vibration reduction immediately raises the question whether such a system could be also used for noise reduction and performance enhancement. Recent studies [13–15] have clearly shown the potential of the ACF system to produce noise reduction as well as simultaneous noise and vibration reduction. Combining noise and vibration reduction with performance enhancement could produce a significant improvement in rotorcraft technology.

This paper has several objectives listed below:

1. Present a concise chronological description of the evolution of the ACF technology.
2. Summarize the essential features of the aeroelastic simulation code developed by the author and his students.
3. Describe the experimental data available that is suitable for validation studies, and describe some important results.
4. Address issues associated with practical implementation of the ACF approach.
5. Describe briefly the noise reduction capability of the ACF system.

Evolution of ACF Concept

The ACF approach was inspired by the early research conducted by Lemnios and Smith [16] who used a servo flap, which is a primary control device on Kaman helicopters, to study the characteristics of a torsionally soft controllable twist rotor (CTR). Using a combination of collective and cyclically varying twist distribution on the blade, they demonstrated a considerable increase in performance and a 30% decrease in blade-bending amplitudes. However, they did not consider the use of the servo flap, as a means for vibration control.

The concept of the ACF for vibration reduction has been first studied by Millott and Friedmann [17-19], who have demonstrated the feasibility of the ACF for vibration reduction using aeroelastic simulation. Spangler and Hall [20] studied the piezoelectric actuation for the ACF as a potential vibration reduction device. However, the actual vibration reduction capability of the device in a rotary wing environment was not considered in Ref. [20].

The first aeroelastic simulation model of an ACF for vibration reduction was developed in the pioneering studies by Millott and Friedmann and was used to demonstrate the effectiveness of the ACF as a vibration reduction device [17-19]. Millott and Friedmann used a coupled flap-lag-torsional isotropic blade model, including geometric nonlinearities due to moderate deflections. Modified quasisteady Theodoresen theory was used to represent the aerodynamic loads for the blade/trailing edge flap combination. Using a simple controller similar to that employed in HHC vibration reduction studies [1], controlled vibration levels comparable to the HHC and conventional IBC methods were obtained. Furthermore, it was shown that the power requirements of the ACF are approximately an order of magnitude smaller than those for conventional IBC.

Following this ground-breaking work, other researchers have also investigated the effectiveness of the ACF as a means of vibration reduction. Milgram and Chopra [21, 22] have developed an aeroelastic model using the University of Maryland's comprehensive rotor analysis code UMARC. Finite elements were used to model the structural dynamic properties of the blade. An unsteady, compressible flow aerodynamic model developed by L-eishmann combined with a free wake model was used to model the airloads. Experimental results from wind tunnel tests of the ACF were also presented [22], the purpose of these early studies was to demonstrate the feasibility and effectiveness of this new approach to vibration control.

The need for an improved aeroelastic simulation model for the flap-blade combination led to the development of new and improved models based on a compressible time domain unsteady aerodynamic model. This simulation capability could accommodate three different flap configurations, including dual flaps. Detailed vibration reduction studies from this model were presented in Refs. [23-27].

Subsequently, this model was improved by adding a free wake model to the time domain unsteady compressible theory [27-30]. The resulting comprehensive simulation model facilitated the examination of two distinctly different flight regimes in which vibrations are reduced using the ACF: a high speed flight regime, where advance ratio effects are dominant and the influence of the free wake is limited, and low or moderate advance ratio regime where blade vortex interactions (BVI) are important. These studies have clearly demonstrated that vibration reduction at low advance ratios ($\mu = 0.15$) is a more demanding control task, due to the presence of BVI, than vibration reduction at high speeds of $\mu = 0.30$ or higher. An early experimental study aimed at determining the feasibility of the ACF concept was conducted at the NASA Langley 14×22 ft subsonic wind tunnel by Straub [31] and Dawson et al [32]. This was an open loop test where flap inputs were limited to single-frequency, fixed amplitude 3/rev and 5/rev inputs. Large changes in individual components of the vibratory response were obtained. However, this single frequency control based on a fixed amplitude input did not produce multicomponent vibration reduction. Much more valuable and fundamental experimental results on the practical implementation of the ACF and its application to vibration reduction in the open loop mode, on a Mach scaled two bladed hingeless rotor, were obtained by Fulton and Ormiston [33]. The tests were conducted in the Ames 7×10 ft wind tunnel, on a 7.5 ft rotor with a 3.4" chord, with a single flap on each blade centered at 75% span. The plain flap had a chord equal to 10% blade chord, and the maximum flap deflections obtained by a piezoelectric bimorph type actuator were approximately 5°at an advance ratio of 0.20. The experimental results obtained in these tests were compared with the experimental simulation described in Ref. [29], and the correlation with the experimental data was found to be quite good, in most cases.

One important issue associated with the implementation of ACF systems to the vibration reduction problem involves saturation. Saturation can be due to limitations associated with piezoelectric actuation which can provide flap deflections of 4°or less. Alternatively, when larger flap deflections are possible, for practical reasons, it is desirable to limit flap authority to 3-4 degrees, so as to avoid interfering with the handling qualities of the helicopter. An effective way of limiting saturation without loss of control effectiveness has been presented by Cribbs and Friedmann [34].

Two additional studies [35,36] have considered the capability of single and dual ACF systems to alleviate vibrations due to dynamic stall at high advance ratios. Furthermore, the effect of freeplay on the vibration reduction effectiveness of the ACF was also studied in Ref. [36]. The effect of dynamic stall was incorporated in the simulation [35] by using the ONERA dynamic stall model and combining it with the unsteady aerodynamics, described in Refs. [26] and [29]. Another important ingredient added in this study was the drag due to the flap deflection [35]. Using a conventional control algorithm, employed in most HHC and IBC studies, it was shown that the ACF flap is very successful in alleviating vibrations due to dynamic stall [35].

An experimental demonstration on the feasibility of using piezoelectrically actuated flaps for vibration reduction in forward flight was conducted by Koratkar and Chopra [37, 38]. The rotor was tested in the University of Maryland wind tunnel. It was a four bladed Mach scaled bearingless rotor resembling a Bell-412, the scale was approximately 1/7th of full scale. The flaps were actuated by piezoelectric benders. When operating in the closed loop mode, a neural network controller was used. Reference [37] describes primarily hover and open loop tests, while Ref. [38] describes the closed loop tests in forward flight. The largest flap deflections reco-rded were in the range of $4^\circ < |\delta_f| < 6^\circ$ for components introduced with frequency of 1, 2, 3, 4, and 5/rev. With this control authority, 70-90% reduction in the vibratory loads was obtained in the advance ratio of $0.10 < \mu < 0.30$ for relatively low thrust coefficient. Comparisons between the experimental data and computer simulation were not presented in the paper.

Numerous other studies on vibration reduction using actively controlled flaps were carried out. Parametric design issues were considered in Ref. [39]. Using an early version of the Maryland comprehensive analysis code UMARC. A partially successful attempt to correlate with the experimental data obtained in Refs. [31] and [32] is described in Ref. [22]. Straub and his coworkers [40] have simulated vibration reduction by an ACF system using the comprehensive analysis code CA-MRAD II [41]. These studies were in support of the development of a full scale rotor test with piezoelectrically actuated flaps.

Other, recent, studies have addressed the issue of individual blade control of a helicopter with dissimilar rotor blades. The blade control is implemented using a conventional HHC algorithm coupled with a refined Kalman filter approach. Actuation is implemented by piezoelectrically driven trailing edge flaps. The controller was shown to reduce successfully the vibratory hub loads due to blade dissimilarities [42].

Numerous studies dealing with the design of actuators for ACF systems were also carried out. A detailed survey paper by Chopra [43] reviews in detail many studies that have attempted to combine piezoelectric actuation with trailing edge flaps for vibration reduction. Other studies have also considered magnetostrictive actuation for the flap [44].

Currently, full scale wind tunnel tests and flight tests of ACF systems are imminent and will be described later in this paper.

Essential Features of the Aeroelastic Simulation Codes

Aeroelastic simulation codes capable of modeling vibration reduction due to an ACF system have to be quite refined in order to provide the level of accuracy required for correlation with experimental data. Furthermore, correlation with experimental data is a necessary requirement for code validation. Such codes usually combine the aeroelastic response analysis available in a modern comprehensive rotorcraft analysis code with a control algorithm that is employed in the vibration reduction process. The description of the simulation capability provided in this paper follows the code developed by the author and his associates. Other simulation codes have very similar ingredients.

Aeroelastic Response Model

Structural Dynamic Model. The structural dynamic model resembles that described in Ref. [19]. The rotor is assumed to be composed of four identical blades, connected to a fixed hub, and it is operating at a constant angular velocity Ω. The hingeless blade is modeled by an elastic beam cantilevered at an offset e from the axis of rotation, as shown in Fig. 4. The blade has fully coupled flap, lead-lag, and torsional dynamics. The strains within the blade are assumed to be small and the deflections to be moderate. The inertia loads are obtained from D'Alembert's principle and an ordering scheme is used to simplify the equations.

The control surfaces are assumed to be an integral part of the blade, attached at a number of spanwise stations. It is assumed that the control surfaces do not modify the structural properties of the blade, only the inertia and aerodynamic loads due to the flaps are accounted for. The control surface is constrained to pure rotation in the plane of the blade cross-section.

Aerodynamic Model for Attached Flow. Blade section aerodynamic loads are calculated using a rational function approximation (RFA) approach described by Myrtle and Friedmann [26]. The RFA approach is an unsteady time-domain aerodynamic theory that accounts

for compressibility, variations in the incoming flow and combined blade, trailing edge flap configuration in the cross-section. These attributes make the RFA model particularly useful when studying vibration reduction in the presence of dynamic stall. The RFA approach generates approximate transfer functions between the generalized motion vector and the generalized attached flow vector.

A non-uniform inflow distribution, obtained from a free wake model is employed. The free wake model has been extracted [28] from the rotorcraft analysis tool CAMRAD/JA [45]. The wake vorticity is created in the flow field as the blade rotates, and then convected with the local velocity of the fluid. The local velocity of the fluid consists of the free stream velocity, and the wake self-induced velocity. The wake geometry calculation proceeds as follows: (1) the position of the blade generating the wake element is calculated, this is the point at which the wake vorticity is created; (2) the undistorted wake geometry is computed as wake elements are convected downstream from the rotor by the free stream velocity; (3) distortion of the wake due to the wake self-induced velocity is computed and added to the undistorted geometry, to obtain a free wake geometry. The wake calculation model [45] is based on a vortex-lattice approximation for the wake.

An approximate methodology for introducing drag corrections due to flap deflections has been described in Ref. [35].

Aerodynamic Model for Separated Flow. The aerodynamic model used for the separated flow is the ONERA dynamic stall model described by Petot in Ref. [46], which is one of the more useful dynamic stall models which provides the aerodynamic load during both attached flow and separated flow. However, in the aeroelastic simulation, only the separated flow portion of the model is used. The model requires 22 empirical coefficients that are determined from parameter identification from experimental measurements on oscillating airfoils. The separation criterion is based on angle of attack. Details on the integration of the model into the simulation code are provided in Refs. [35] and [36].

Combined Aerodynamic Model. The complete aerodynamic model used in this study consists of the RFA model for attached flow loads, using a free wake model in order to obtain the non-uniform inflow. The ONERA dynamic stall model is used for separated flow loads. Thus the complete aerodynamic state vector for each blade section consists of RFA attached flow states and ONERA separated flow states, together with the representation of the free wake.

Method of Solution

The blade is discretized [19] using the global Galerkin me-thod, based upon the free vibration modes of the rotating blade. Three flapping modes, two lead-lag modes and two torsional modes are used in the actual implementation. The combined structural and aerodynamic equations form a system of coupled differential equations that can be cast in state variable form. They are then integrated in the time domain using the Adams-Bashfort DE/STEP predictor-corrector algorithm. The trim procedure [27] enforces three force equilibrium equations (longitudinal, vertical and lateral forces) and three moment equilibrium equations (roll, pitch and yaw moments). A simplified tail rotor model is used, using uniform inflow and blade element theory. The six trim variables are the rotor shaft angle α_R, the collective pitch θ_0, the cyclic pitch θ_{1s} and θ_{1c}, the tail rotor constant pitch θ_t and the lateral roll angle ϕ_R. The trim procedure is based on the minimization of the sum J_R of the square of trim residuals. At high advance ratios ($0.30 < \mu \leq 0.35$) in the presence of dynamic stall, an autopilot procedure described in Ref. [47] is used to accelerate convergence to the trim state. At higher advance ratios ($0.35 < \mu$), an iterative optimization program based on Powell's method is used to find the trim variables that minimize J_R.

Control Approach and Algorithm

The control of vibrations is implemented either as a single actively controlled partial span trailing edge flap, or in a dual configuration shown in Fig.1. Each flap is independently controlled, and the controller is aimed at reducing the 4/rev vibratory hub shear and moments, in the fixed system. The control strategy is based on the minimization of a performance index [1, 2, 19, 27] that is a quadratic function of the vibration magnitudes $\mathbf{z}_i$ and control input amplitudes $\mathbf{u}_i$:

$$J = \mathbf{z}_i^T \mathbf{W}_z \mathbf{z}_i + \mathbf{u}_i^T \mathbf{W}_u \mathbf{u}_i \tag{1}$$

The subscript i refers to the i-th control step, reflecting the discrete-time nature of the control. The time interval between each control step must be long enough to allow the system to return to the steady state so that the 4/rev vibratory magnitudes can be accurately measured. The matrices $\mathbf{W}_z$ and $\mathbf{W}_u$ are weighting matrices on the vibration magnitude and control input, respectively.

A linear, quasistatic, frequency domain representation of the vibratory response to control inputs is used. The input harmonics are related to the vibration components through a transfer matrix $\mathbf{T}$, given by

$$\mathbf{T} = \frac{\partial \mathbf{z}_i}{\partial \mathbf{u}_i} \tag{2}$$

The optimal control is:

$$\mathbf{u}_i^* = -\mathbf{D}^{-1}\mathbf{T}^T\{\mathbf{W}_z\mathbf{z}_{i-1} - \mathbf{W}_z\mathbf{T}\mathbf{u}_{i-1}\} \qquad (3)$$

where

$$\mathbf{D} = \mathbf{T}^T\mathbf{W}_z\mathbf{T} + \mathbf{W}_u \qquad (4)$$

This algorithm is usually denoted as the conventional higher harmonic control (HHC) algorithm, which is essentially a disturbance rejection algorithm. Despite its relative simplicity this algorithm has performed well in most vibration reduction studies. Recently this algorithm has undergone rigorous re-examination from a control theory-oriented perspective [48]. In Ref. [48] improved adaptive version of the algorithm using online identification is developed together with relaxed version of the HHC algorithm which is much more robust than the classical algorithm.

In the practical implementation of the ACF, adaptive materials based actuation, using piezoelectric or magnetostrictive materials, has been extensively studied. A-daptive materials are limited in their force and stroke producing capability, leading to fairly small angular deflections. From a control perspective, this leads to saturation which introduces serious problems for vibration control. This important problem was studied and solved effectively in a recent paper by Cribbs and Friedmann [34]. This approach to dealing with saturation, is also used in this paper. Saturation is treated by the auto weight approach [34]. The weighting matrix $\mathbf{W}_u$ is represented by a form which allows its modification by premultiplying by a scalar c_{wu} that is continuously adjusted. The controller manipulates the scalar multiplier to provide the proper flap constraints. If the flap deflection is overconstrained, the controller reduces the value of c_{wu} and a new optimal control is calculated. If the flap deflection is underconstrained, the controller increases the value of c_{wu} and a new optimal control is calculated. The iterative procedure reduces or increases c_{wu} until the optimal control converges to the desired deflection limits with a prescribed tolerance. The control input $\mathbf{u}_i$ is given by the flap angle δ which is a sum of four harmonics

$$\delta(\psi_k) = \sum_{N=2}^{5} [\delta_{Nc}\cos(N\psi_k) + \delta_{Ns}\sin(N\psi_k)] \qquad (5)$$

where δ_{Nc} and δ_{Ns} are the cosine and sine components of the N/rev control input.

Freeplay Model. Freeplay can also be implemented in the model as shown in detail in Ref. [36].

Selected Results for Vibration Reduction

Numerous simulations of the effectiveness of the ACF system to reduce vibration have been carried out in the studies described in Section 2 of this paper. Many studies dealt with either hingeless or bearingless rotors. Thr-ee control surface configurations depicted in Fig. 4 have been considered. The first is a servo flap configuration that was the earliest configuration studied, the next one is a plain flap configuration and the last one is a dual servo flap configuration. Obviously, the dual flap configuration can also be implemented using the plain flap. Several studies were also conducted to determine the location of the ACF. For the single flap configuration, it was found that centering the flap at 75% of the blade span produces almost optimal performance for many cases [19]. The basic difference between the plain flap and the servo flap is that for the plain flap, the control surface is an integral part of the blade, resulting in a cleaner low drag implementation when compared to the servo flap. Many of the simulations performed were done on a four bladed hingeless rotor that resembles a MBB BO-105 type rotor for which the basic data on the single and dual flap configurations is given in Tables 1 and 2. From the numerous results generated on the ACF, some of the most important results and conclusions are concisely summarized in this section.

Early research on a single servo flap ACF system [1, 6, 17, 19] has demonstrated that the power requirements of the ACF are approximately an order of magnitude lower than root actuated conventional IBC for blades that are torsionally soft, i.e. $\omega_{T1} < 4.0$. Also, the vibration reduction effectiveness of the ACF is reduced when the torsional stiffness of blade increases to $\omega_{T1} = 6.0$ or higher. Furthermore, detailed results shown in Ref. [27] have shown that the vibration reduction effectiveness of the servo flap is considerably better than the plain flap, and the effectiveness of the dual servo flap is the best.

It was also found that the mechanism of vibration reduction at low advance ratios, where blade vortex interaction (BVI) dominates, is fundamentally different from the mechanism of vibration reduction at higher advance ratios, $\mu = 0.30$ or higher. This behavior is illustrated in Figs. 5-7 which describe vibration reduction and the flap deflection history for the two advance ratios. The blade dynamics in these results are all modeled with 3 flap, 2 in-plane, one torsional and one axial mode. The helicopter is in trimmed level flight with a weight coefficient of $C_W = 0.00515$, which is approximately equal to the thrust coefficient [27, 29, 30].

Using the actively controlled flap, simultaneous reduction of 4/rev vibratory hub shears and moments with the nonuniform inflow free wake model was studied. Results were generated for two advance ratios, $\mu = 0.15$ and $\mu = 0.30$. These two cases correspond to two different vibration problems caused by different phenomena. At $\mu = 0.15$, the effects of BVI are strong and represent a major source of higher harmonic airloads,

while at $\mu = 0.30$, BVI is less significant and vibratory loads are mostly due to the high forward flight velocity. As indicated previously, the control law for the flap consists of a combination of 2, 3, 4, and 5/rev harmonic input frequencies. The results from this study are shown in Figs. 5-12. Figures 5 and 6 show the baseline and controlled vibratory loads. The local controller is effective at reducing the vibratory loads at both advance ratios, but its performance at $\mu = 0.15$ is not as good as at $\mu = 0.30$. This is to be expected, since at $\mu = 0.30$, the effects of nonuniform flow are mild, and earlier results indicated that the actively controlled flap performed very well when uniform inflow distribution is assumed. The favorable results obtained for the case of $\mu = 0.15$ indicate that the actively controlled flap is a viable device for alleviating BVI effects at low advance ratios. Figures 7 and 8 illustrate the flap input and its harmonic content for the two cases. The figures emphasize the difference between the flap input at the two advance ratios, indicating that the vibratory loads for the two cases are very different. It should also be noted that for $\mu = 0.15$, considerably larger flap deflections are needed for vibration alleviation. Also, it is important to note that the 2/rev components play a more significant role in the case of BVI alleviation than it does at high advance ratios.

Figures 9-12 show the nondimensional tip deflections in the flap and torsional degrees of freedom. These plots provide insight on the operation of the controller and the mechanism of vibration reduction. From Fig. 10, it is clear that the actively controlled flap does not modify significantly the flapwise dynamics of the blade for the $\mu = 0.30$ case, while it does so at $\mu = 0.15$ as indicated in Fig. 9. This implies that two different strategies are employed by the controller to tackle the vibration alleviation problem at the different advance ratios. At high advance ratio, $\mu = 0.30$, the normal flapping dynamics of the blade results in a redistribution of the aerodynamic loads over the azimuth. Whereas at $\mu = 0.15$, the controller drives the blade into a region of large flapping dynamics that modifies the relative spacing between the blade and the tip vortices and reduces BVI. These results suggest that the control of BVI induced vibration requires a more refined control strategy where additional variables such as blade-vortex spacing should be included in the objective function. Figures 11 and 12 indicate that blade torsional deflections are also amplified as a result of the controlled flap activity, particularly at the lower advance ratio. This is not surprising since the flap and torsional degrees of freedom have considerable structural coupling.

Inspection of Fig. 7 shows that for BVI alleviation fairly large control angles are required, and for practical implementation of ACF systems, it is essential to limit flap deflections to 5°or less. This requirement placed an emphasis on issues associated with control saturation that have been treated in detail in Ref. [34], where three different methods for constraining flap deflections were studied. It was shown that intuitive limits such as scaling or clipping of the optimal control deflection to a given maximum value introduce severe degradation in the vibration reduction effectiveness of the ACF system. A new control procedure, for modifying the weighting matrix associated with the control effort was developed and it was shown that flap deflection can be limited to a desired value without any significant degradation in controller performance.

An important issue associated with codes which can simulate vibration reduction achieved by ACF system, is the validation of the code with experimental data available. The simulation code developed by the author and his associates [29] was validated by comparing it with experimental data obtained by Fulton and Ormiston [33]. The experiments were conducted on a two bladed hingeless rotor at an advance ratio of $\mu = 0.20$. The rotor was excited by piezoelectrically activated plain flap inputs at 2, 3, 4, and 5/rev. The magnitude of the flap input was $\delta_f = 5^\circ$, and the flap was operated in the open loop mode. The purpose of the experiment was not to reduce vibrations, but to excite the blade dynamics with the flap and thus determine its control authority. The root flapping moment of the blade was measured. These flapping moments were also simulated by the code. Results are shown in Figs. 13 and 14, Fig. 13 shows the response due to the 2/rev excitation and Fig. 14 shows the response due to 3/rev excitation. The two blades tested were not identical, and therefore each plot contains two sets of experimental data, one for Blade 1 and another for Blade 2, respectively. The simulations were conducted for an average blade and the results are shown by the triangles in Figs. 13 and 14. Clearly, the agreement between the simulation and the test is quite good.

As evident from the results that have been presented at low advance ratios, BVI is an important effect that generates large vibratory hub shears and moments. On the other hand, in high speed flight, high vibratory loads are induced by dynamic stall. A detailed study of alleviation of vibratory loads, due to dynamic stall by using an ACF system has been completed recently [35, 36]. The effect of dynamic stall was incorporated in the simulation [35] using the ONERA dynamic stall model and combining it with the unsteady aerodynamic model, described in Refs. [29] and [30]. The drag due to flap deflections was also incorporated in this study in an approximate manner. Using the control algorithm described earlier, together with the saturation limiting scheme [34], it was shown that the ACF can significantly alleviate the vibrations due to dynamic stall. The vibration reduction obtained is shown in Fig. 15 for both a single flap and a dual flap configuration. In

both cases, saturation limits, limiting flap deflections to $-4^\circ < \delta_f < 4^\circ$ were imposed. The vibration reduction effectiveness of the dual flap configuration is better than that of the single flap configuration. Results not shown here indicate that the flap deflections can introduce a rotor power penalty due to drag of approximately 2%. The power needed to actuate the flaps is quite low and it represents less than 0.01% of rotor power.

Another recent study [49] has examined helicopter vibration reduction using both single, dual and multiple (i.e. triple) trailing edge flaps controlled by a resonance actuation system. Using simulation it was shown that the multiple actively controlled trailing edge system, based upon three plain flaps (see Fig. 4) centered at 0.635R, 0.735R and 0.935R respectively, with a span of 0.07R each, could outperform both the single and dual flap configurations for vibration suppression. While it is interesting to see that multiple flap systems appear to be the best, the mechanical complexity associated with installing three flap systems on a blade has been disregarded in this study.

Full Scale Implementation of the ACF Approach

Full scale implementation of the ACF approach has been developed for an MD-900 Explorer as part of the Smart Rotor demonstration program funded by DARPA [40]. The rotor is a 5 bladed bearingless rotor with a 34ft diameter. The ACF system is implemented by using the single plain flap configuration with piezoelectric actuation provided by the piezo-stack driven X-frame actuator developed by Prechtl and Hall [50]. To obtain bi-directional operation, the blades are equipped with dual X-frame actuators. The flap used has a span of 18% of blade length and its chord is 25% of the blade chord, and it is centered at 83% of the blade radius. Initially, a complete flight test of this experimental helicopter was planned. However, funding shortages caused the flight test program to be replaced with a combination of whirl tower testing and wind tunnel testing in the NASA Ames 40×80ft wind tunnel. These tests are scheduled to take place in 2003.

A full scale rotor based on a hingeless BK 117/EC 145 is also under development in Europe [51, 52]. The rotor blades have been bench tested, and preliminary tests have also been carried out on the whirl tower to confirm the dynamic layout and the aerodynamic efficiency of the ACF system. The flap system consists of three identical units with an individual length of 0.3m each, and the three units are adjacent to each other. Each unit represents a plain flap. The units are centered at $0.718R$, $0.773R$, and $0.827R$, they span 16% of the blade radius between the radial station 3.8m and 4.7m, and the total rotor radius is 5.5m. The flap chord is 15% of the blade chord, and the flaps are designed to operate between $-10^\circ < \delta_f < 10^\circ$. The controller is designed to provide the flaps with a combination of 2, 3, 4, and 5/rev, as indicated in Eq. (5). The flight tests are supposed to take place in 2004, and the designers claim that this ACF system is the only active control technology capable of simultaneous reduction of exterior noise and cabin vibrations.

Noise Reduction Using the ACF Approach

As indicated in the introduction recent research has shown that the ACF system has considerable potential as a means for reducing noise due to BVI [13–15]. As shown in these studies [13–15] attempts to reduce noise by active control frequently cause increased vibration levels and vice-versa. Only in a few isolated cases was simultaneous vibration and noise reduction demonstrated using HHC in a wind tunnel test.

In Refs. [13–15], the aeroelastic simulation capability for vibration reduction using single and dual ACF systems described earlier in this paper has been extended so as to simulate noise generation under BVI conditions in descent. The primary changes introduced in the simulation are described in detail in Ref. [13] and are summarized below:

(a) The RFA unsteady compressible aerodynamic module [26] was modified so as to produce a chordwise unsteady pressure distribution, in addition to the cross sectional unsteady lift and moment.

(b) The free wake model used in the simulation was refined to provide a 2°azimuthal wake resolution.

(c) The free wake model that was originally taken from CAMRAD/JA was modified by incorporating a second inboard vortex line. This feature of the wake model becomes active only when the tip loading becomes negative. The free wake distortion computation routine was also modified to include the deformation of this second inboard vortex line.

(d) The unsteady pressure on the surface of the blade is used to provide input to a modified version of the WOPWOP code. The modifications to the WOPWOP code consist of the replacement of the original blade model with a fully flexible blade model with coupled flap-lag-torsional dynamics, undergoing moderate deflections.

The control algorithm was also modified as described in Ref. [15]. For BVI noise reduction the vector $\mathbf{Z}_i$ in

Eq.(1) is replaced by the vector

$$\mathbf{z}_{k,\mathrm{NR}} = \left\{ \begin{array}{c} N_{H06} \\ \vdots \\ N_{H17} \end{array} \right\} \tag{6}$$

$\mathbf{z}_{k,\mathrm{NR}}$ from Eq.(6) which includes acoustic pressure levels in the $6^{th} - 17^{th}$ harmonics of the blade passage frequency measured by a microphone located on the skid of the helicopter, as shown in Figure 16.

For simultaneous reduction of vibration and noise a combined vector is used

$$\mathbf{z}_{k,\mathrm{SR}} = \left\{ \frac{\mathbf{z}_{k,\mathrm{VR}}}{\mathbf{z}_{k,\mathrm{NR}}} \right\}. \tag{7}$$

where $\mathbf{z}_{k,\mathrm{VR}}$ contains the usual hub shears and moments used in the vibration reduction problem. Thus $\mathbf{z}_{k,\mathrm{SR}}$ is simply a partitioned combination of hub shear and noise levels. The weighting matrix $\mathbf{W}$ (see Eq. 1) is used to adjust the control effort so as to achieve a desirable balance between vibration and noise reduction levels.

Before showing noise and vibration reduction results it is important to mention that the extended noise and vibration simulation code has been carefully correlated against HART data, as shown in Refs. [14] and [15].

Simultaneous noise and vibration reduction with this code has been demonstrated in Ref. [15], for a helicopter resembling an MBB BO-105, at an advance ratio of $\mu = 0.15$, a -6 degree descent angle, and a weight coefficient of $C_W = 0.005$. In the weighting matrix the noise components were weighted 10 times larger than the vibration components. Results are shown in Fig. 17 for vibration reduction and Fig. 18 for noise reduction, for both the single flap and the dual flap ACF configurations. The results are present for both no saturation limits on the flap, as well as 4° degree saturation limits.

In Fig. 17 it is shown that in absence of saturation limits the single ACF reduces the vertical hub shear by 71%, and the dual ACF produces a 80% reduction in the vertical component. These reductions in the 4/rev vertical hub shears are similar to the results obtained when only vibration levels were reduced. However, when saturation limits and the modified weighting are introduced, the vibration levels are reduced by 38% and 36% for the single and dual flap respectively.

Figure 18 shows the noise carpet plot reductions compared to the baseline. The noise at the feedback location SKID1 was decreased by $2dB$ and $3dB$, for the single and dual flap configurations without saturation limits, respectively. With saturation limits and modified weighting, these decreases are $3dB$ and $4dB$ for single and dual flaps, respectively. This reflects upon the increased emphasis on noise reduction. The noise levels on the carpet plot are shown in Figs 18b through 18e. For the single flap, Fig 18b, without saturation, no significant noise reduction occurs, although the noise directivity pattern is slightly modified. However, with dual flaps, reductions of $3-5dB$ are found on the advancing side, without noticeable increases on the retreating side, as shown in Fig 18c. With modified weighting and saturation limits, reductions of $4-5dB$ for the single flap case and $5-6dB$ for the dual flap case are obtained on the retreating side. The improved noise reduction found with saturation limit corresponds to the different weighting matrix used.

Concluding Remarks

This paper provides a detailed description of the evolution of the actively controlled flap technology together with the essential features of the aeroelastic simulation codes needed for predicting the behavior of ACF systems. A representative simulation code is validated agai-nst experimental data. It is shown that ACF technology is capable of alleviating BVI induced vibration, as well as vibrations due to high speed flight and dynamic stall. Based on current data, the ACF system implemented in the dual flap configuration appears to offer the best solution for overall vibration reduction. Furthermore as shown in Refs [14] and [15] simulteneous noise and vibration reduction has been also demonstrated in the simulations conducted. Two additional advantages of the ACF systems are: (1) low power requirements for its operation, and (2) no effect on the airworthiness of the helicopter. Full scale implementations of this approach are imminent in Europe. It is therefore expected that this particular implementation of IBC technology will become sufficiently mature and reliable, so as to warrant implementation in a production helicopter.

Clearly if the vibration and noise reduction capability of the ACF system can be augmented by performance enhancement, then the ACF system will succeed in making significant improvements in rotorcraft technology.

Acknowledgment

This research was supported in part by the ARO Grant 02-1-0202 with Dr. G. Anderson as grant monitor. Partial support by the FXB Center for Rotary and Fixed Wing Air Vehicle Design is also gratefully acknowledged.

REFERENCES

1. Friedmann, P.P., and Millott, T.A., "Vibration Reduction in Rotorcraft Using Active Control: A Comparison of Various Approaches," *AIAA Journal of Guidance, Control and Dynamics*, Vol. 18, July-August 1995, pp. 664 – 673.

2. Johnson, W., "Self-Tuning Regulators of Multicyclic Control of Helicopter Vibrations," NASA, TP 1996, 1982.

3. Wood, E.R., Powers, R., Cline J.H., and Hammond, C.E., "On Developing and Flight Testing a Higher Harmonic Control System," *Journal of the American Helicopter Society*, Vol. 30, No. 1, 1985, pp. 3 – 20.

4. Polychroniadis, M. and Achache, M., "Higher Harmonic Control: Flight Tests of an Experimental system on SA349 Research Gazelle," *Proceedings of the 42nd Annual Forum of the American Helicopter Society*, Vol. 2, Washington, DC, 1986, pp. 811 – 820.

5. Robinson, L.H. and Friedmann, P.P., "A Study of Fundamental Issues in Higher Harmonic Control Using Aeroelastic Simulation," *Journal of the American Helicopter Society*, Vol. 36, No. 2, 1991, pp. 32 – 43.

6. Millott, T.A. and Friedmann, P.P., "Vibration and Reduction in Hingeless Rotors Using an Actively Controlled Trailing Edge Flap: Implementation and Time Domain Simulation," *Proceedings of the 35th AIAA/ASME/ASCE/AHS/ASC Structures, Structural Dynamics and Materials Conference*, Hilton Head, SC, April 18-20 1994, pp. 9 – 22.

7. Cesnik, C.E.S., Shin, S., Wilbur, M.L., and Wilkie, W.K., "Design and Testing of the NASA/Army/MIT Active Twist Prototype Blade," *Proceedings of the 26th European Rotorcraft Forum*, The Hague, The Netherlands, September 26-29 2000, pp. 17.1 – 17.11.

8. Wilkie, W.K., Wilbur, W.M., Mirick, P.H., Cesnik, C.E.S., and Shin, S., "Aeroelastic Analysis of the NASA/Army/MIT Active Twist Rotor," *Proceedings of the 55th Annual Forum of the American Helicopter Society*, Montreal, Canada, May 25-27 1999.

9. Jacklin, S.A., Blass, A., Teves, D., and Kube, R., "Reduction of Helicopter BVI Noise, Vibration and Power Consumption through Individual Blade Control," *Proceedings of the 51st Annual Forum of the American Helicopter Society*, Ft. Worth, TX, 1995.

10. Schimke, D., Arnold, T.P., and Kube, R., "Individual Blade Root Control Demonstration - Evaluation of Recent Flight Test," *Proceedings of the 54th Annual Forum of the American Helicopter Society*, Washington, DC, May 1998.

11. Cribbs, R.C., Friedmann, P.P., and Chiu, T., "Coupled Helicopter Rotor/Flexible Fuselage Aeroelastic Model for Control of Structural Response," *AIAA Journal*, Vol. 38, October 2000, pp. 1777 – 1788.

12. Cribbs, R.C. and Friedmann, P.P., "Vibration Reduction in Rotorcraft Using an Enhanced ACSR Model," AIAA Paper No. 2000-1687, *Proceedings of the AIAA/ASME/ASCE/AHS/ASC 41st Structures, Structural Dynamics and Materials Conference*, Atlanta, GA, April 3-6 2000.

13. Patt, D., Liu, L., and Friedmann, P.P., "Rotorcraft Vibration Reduction and Noise Prediction Using an Unified Aeroelastic Response Simulation," *Proceedings of the 59th Annual Forum of the American Helicopter Society*, Phoenix, AZ, May 6-8 2003.

14. L. Liu, D. Patt, and P. P. Friedmann, "Simultaneous Vibration and Noise Reduction in Rotorcraft Using Aeroelastic Simulation," *Proceedings of the 60th American Helicopter Society Annual Forum*, Baltimore, MD, June 7-10 2004.

15. D. Patt, L. Liu, and P. P. Friedmann, "Achieving Simultaneous Reduction of Rotorcraft Vibration and Noise Reduction Using Simulation," *Proceedings of the 30th European Rotorcraft Forum*, Marseille, France, September 14-16 2004.

16. Lemnios, A.Z., and Smith, A.F., "An Analytical Evaluation of the Controllable Twist Rotor Performance and Dynamic Behavior," Kaman, TR R-794, 1972.

17. Millott, T.A., and Friedmann, P.P., "Vibration Reduction in Helicopter Rotors Using an Active Control Surface Located on the Blade," AIAA Paper 92-2451, *Proceedings of 33rd Structures, Structural Dynamics, and Materials Conference*, Dallas, TX, April 1992, pp. 1974 – 1988.

18. Millott, T., and Friedmann, P.P., "The Practical Implementation of an Actively Controlled Flap to Reduce Vibrations in Helicopter Rotors," *Proceedings of the 49th Annual Forum of the American Helicopter Society*, St. Louis, MO, May 1993, pp. 1079 – 1092.

19. Millott, T.A., and Friedmann, P.P., "Vibration Reduction in Helicopter Rotors Using an Actively Controlled Partial Span Trailing Edge Flap Located on the Blade," NASA, CR 4611, June 1994.

20. Spangler, R.L., and Hall, S., "Piezoelectric Actuators for Helicopter Rotor Control," AIAA Paper 90-1076 CP, *Proceedings 31st AIAA/ASME/ASCE/AHS/ACS Structures, Structural Dynamics, and Materials Conference*, Long Beach, CA, April 1990, pp. 1589 – 1599.

21. Milgram, J. and Chopra, I., "Helicopter Vibration Reduction with Trailing Edge Flaps," *Proceedings of the 36th AIAA/ASME/ASCE/AHS/ASC Structures, Structural Dynamics and Materials Conference*, New Orleans, LA, 1995.

22. Milgram, J., Chopra, I., and Straub, F.K., "A Comprehensive Rotorcraft Aeroelastic Analysis with Trailing Edge Flap Model: Validation with Experimental Data," *52nd Annuual Forum of the American Helicopter Society*, Washington, DC, June 4-6 1996, pp. 715 – 725.

23. Myrtle, T.F., "Development of an Improved Aeroelastic Model for the Investigation of Vibration Reduction in Helicopter Rotors Using Trailing Edge Flaps," Ph.D. Dissertation, Mechanical and Aerospace Engineering Dept., University of California, Los Angeles, CA, June 1998.

24. Myrtle, T.F., and Friedmann, P.P., "Unsteady Compressible Aerodynamics of a Flapped Airfoil with Application to Helicopter Vibration Reduction," AIAA Paper 97-1083-CP, *Proceedings of the 38th AIAA/ASME/ASCE/AHS Structures, Structural Dynamics and Materials Conference*, Kissimmee, FL, April, 7-10 1997, pp. 224 – 240.

25. Myrtle, T.F., and Friedmann, P.P., "Vibration Reduction in Rotorcraft Using the Actively Controlled Trailing Edge Flap and Issues Related to Practical Implementation," *Proceedings of the 54th Annual Forum of the American Helicopter Society*, Washington, DC, May, 20-22 1998.

26. Myrtle, T.R. and Friedmann, P.P., "Application of a New Compressible Time Domain Aerodynamic Model to Vibration Reduction in Helicopters Using An Actively Controlled Flap," *Journal of the American Helicopter Society*, Vol. 46, January 2001.

27. Friedmann, P.P., de Terlizzi, M., and Myrtle, T.F., "New Developments in Vibration Reduction with Actively Controlled Trailing Edge Flaps," *Mathematical and Computer Modeling*, Vol. 33, April 2001, pp. 1055 – 1083.

28. de Terlizzi, M. and Friedmann, P.P., "Aeroelastic Response of Swept-Tip Rotors Including the Effects of BVI," *Proceedings of the 54th Annual Form of the American Helicopter Society*, Washington, DC, May 1998, pp. 644 – 663.

29. de Terlizzi, M. and Friedmann, P.P., "Active Control of BVI Induced Vibrations using a Refined Aerodynamic Model and Experimental Correlation," *Proceedings of the 55th Annual Forum of the American Helicopter Society*, Montreal, Canada, May 25-27 1999.

30. de Terlizzi, M. and Friedmann, P.P., "Active Control of Vibrations due to BVI and Experimental Correlation," *Proceedings of the 25th European Rotorcraft Forum*, Rome, Italy, September 14-16 1999, pp. G6.1 – G6.16.

31. Straub, F.K., "Active Flap Control for Vibration Reduction and Performance Improvement," *Proceedings of the 51st American Helicopter Society Forum*, Fort Worth, TX, 1995, pp. 381 – 392.

32. Dawson, S., Marcelini, M., Booth, E., Straub, F., Hassan, A., Tadghighi, H., and Kelly, H., "Wind Tunnel Test of an Active Flap Rotor: BVI Noise and Vibration Reduction," *Proceedings of the 51st Annual Forum of the American Helicopter Society*, Ft. Worth, TX, May 9-11 1995, pp. 631 – 648.

33. Fulton, M. and Ormiston, R.A., "Small-Scale Rotor Experiments with On-Blade Elevons to Reduce Blade Vibratory Loads in Forward Flight," *Proceedings of the 54th Annual Forum of the American Helicopter Society*, Washington, DC, May 20-22 1998, pp. 433 – 451.

34. Cribbs, R.C. and Friedmann, P.P., "Actuator Saturation and Its Influence on Vibration Reduction by Actively Controlled Flaps," AIAA Paper 2001-1467, *Proceedings of the 42nd AIAA/ASME/ASCE/AHS/ASC Structures, Structural Dynamics and Materials Conference*, Seattle, WA, April 16-19 2001.

35. Depailler, G. and Friedmann, P.P., "Alleviation of Dynamic Stall Induced Vibrations Using Actively Controlled Flaps," *Proceedings of the 58th Annual Forum of the AHS*, Montreal, Canada, June 11-13 2002.

36. Depailler, G. and Friedmann, P.P., "Alleviation of Dynamic Stall Induced Vibrations Using Actively Controlled Flaps with Freeplay," Paper No. 45, *Proceedings of the 28th European Rotorcraft Forum*, Bristol, U.K., September 17-20 2002.

37. Koratkar, N.A. and Chopra, I., "Wind Tunnel Testing of a Mach Scaled Rotor Model with Trailing-Edge Flaps," *Journal of Smart Materials and Structures*, Vol. 10, 2001, pp. 1 – 14.

38. Koratkar, N.A. and Chopra, I., "Wind Tunnel Testing of a Smart Rotor Model with Trailing-Edge Flaps," *Journal of the American Helicopter Society*, Vol. 47, October 2002, pp. 263 – 272.

39. Milgram, J., and Chopra, I., "A Parametric Design Study for Actively Controlled Trailing Edge Flaps," *Journal of the American Helicopter Society*, Vol. 43, April 1998, pp. 110 – 119.

40. Straub, F. and Charles, B.D., "Aeroelastic Analysis of Rotors with Trailing Edge Flaps Using Comprehensive Codes," *Journal of the American Helicopter Society*, Vol. 46, July 2001, pp. 192 – 199.

41. Johnson, W., *CAMRAD II, Comprehensive Analytical Model of Rotorcraft Aerodynamics and Dynamics*, Johnson Aeronautics, Palo Alto, CA, 1992-1997.

42. Roget, B. and Chopra, I., "Methodology for Individual Blade Control of Helicopter with a Dissimilar Rotor," Paper No. 32, *Proceedings of the 28th European Rotorcraft Forum*, Bristol, U.K., September 17-20 2002.

43. Chopra, I., "Status of Application of Smart Structures Technology to Rotorcraft Systems," *Journal of the American Helicopter Society*, Vol. 45, October 2000, pp. 228 – 252.

44. Friedmann, P.P., Carman, G.P., and Millot, T.A., "Magnetostrictively Actuated Control Flaps for Vibration Reduction in Helicopter Rotors - Design Considerations for Implementation," *Mathematical and Computer Modeling*, Vol. 33, 2001, pp. 1203 – 1217.

45. Johnson, W., *A Comprehensive Analytical Model of Rotorcraft Aerodynamics and Dynamics, Vol. I: Theory Manual*, Johnson Aeronautics, Palo Alto, CA, 1988.

46. Petot, D., "Differential Equation Modeling of Dynamic Stall," *La Recherche Aerospatiale*, Vol. 5, 1989, pp. 59 – 71.

47. Peters, D.A., Bayly, P., and Li, S., "A Hybrid Periodic Shooting, Auto-Pilot Method for Rotorcraft Trim Analysis," *52nd Annual Forum of the American Helicopter Society*, Washington, DC, June 4-6 1996, pp. 780 – 794.

48. D. Patt, L. Liu, J. Chandrasekar, D. S. Bernstein, and P. P. Friedmann, "The HHC Algorithm for Helicopter Vibration Reduction Revisited," *AIAA Paper No. 2004-1948. Proceedings of the 45th AIAA/ASME/ASCE/AHS/ACS Structures, Structural Dynamics and Materials Conference*, Palm Springs, CA, Apr. 2004.

49. J. Kim, E. C. Smith, and K. W. Wang, "Helicopter Vibration Suppression via Multiple Trailing Edge Flaps Controlled by Resonance Actuation System," *Proceedings of the 60th Annual Forum of the American Helicopter Society*, Baltimore, MD, June 7-10 2004.

50. Prechtl, E.F. and Hall, S.R., "Design of a High Efficiency, Large Stroke, Electromechanical Actuator," *Smart Materials and Structures*, Vol. 8, No. 1, 1999, pp. 13 – 30.

51. Toulmay, F., Kloppel, V., Lorin, F., Enekl, B., and Gaffiero, J., "Active Flaps - The Needs and Current Capabilities," *Proceedings of the 57th Annual Forum of the American Helicopter Society*, Washington DC, May 9-11 2001.

52. Enekl, B. and Kloppel, V., "Full Scale Rotor with Piezoelectric Actuated Blade Flaps," Paper No. 89, *Proceedings of the 28th European Rotorcraft Forum*, Bristol, U.K., September 17-19 2002, pp. 89.1 – 89.14.

Table 1: Elastic blade configuration.

Rotor Data	
N_b=4	
$c_b = 0.005498L_b$	
$\omega_{F1} = 1.123$	$C_{do} = 0.01$
$\omega_{L1} = 0.732$	$C_{mo} = 0.0$
$\omega_{T1} = 3.17$	$a_o = 2\pi$
$\gamma = 5.5$	$\sigma = 0.07$
Helicopter Data	
$C_W = 0.00515$	
$X_{FA} = 0.0$	$Z_{FA} = 0.3$
$X_{FC} = 0.0$	$Z_{FC} = 0.3$

Table 2: Flap configurations.

c_{cs}=$0.25c_b$	
Single flap	
x_{cs}=$0.75L_b$	L_{cs}=$0.12L_b$
Dual flap	
$x^1_{cs} = 0.72L_b$	$L^1_{cs} = 0.06L_b$
$x^2_{cs} = 0.92L_b$	$L^2_{cs} = 0.06L_b$

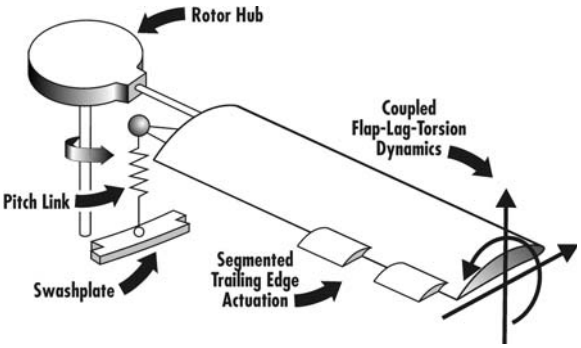

Figure 1. Single or dual ACF configuration used for vibration reduction.

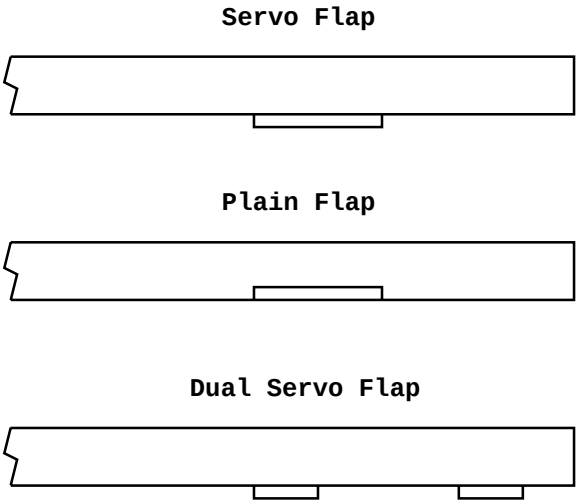

Figure 4. Three control surface configurations investigated.

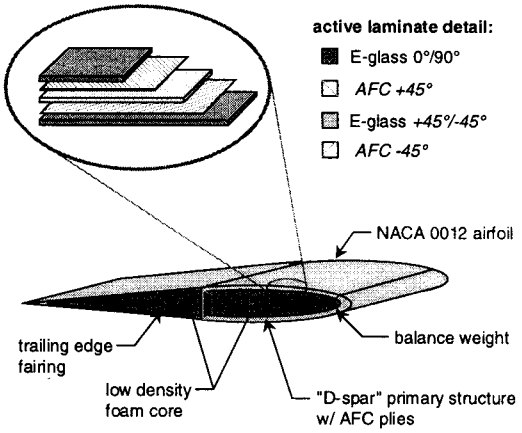

Figure 2. ATR spar structure with active laminates containing piezoelectric fibers.

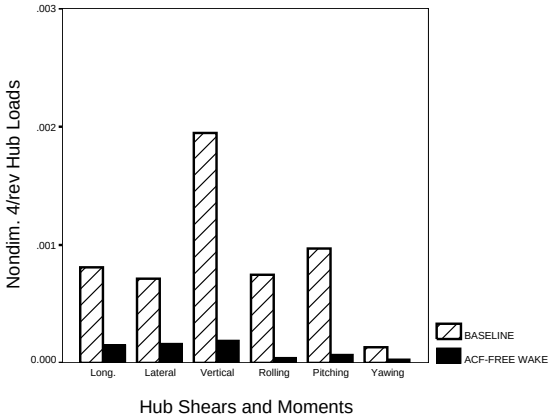

Figure 5. Simultaneous reduction of the 4/rev hub shears and moments, $\mu = 0.15$.

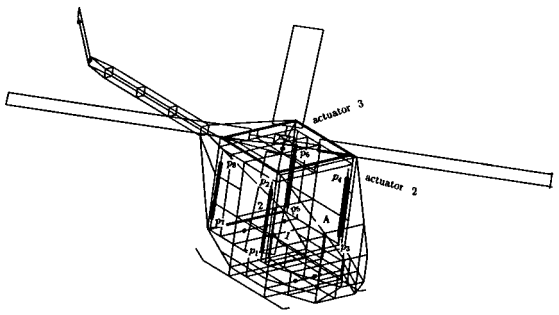

Figure 3. Coupled rotor/flexible fuselage model using ACSR platform and actuators.

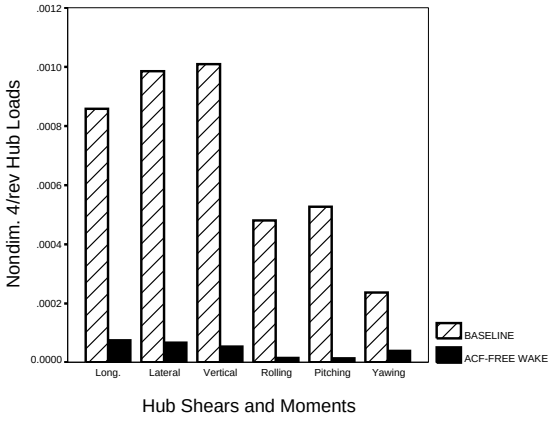

Figure 6. Simultaneous reduction of the 4/rev hub shears and moments, $\mu = 0.30$.

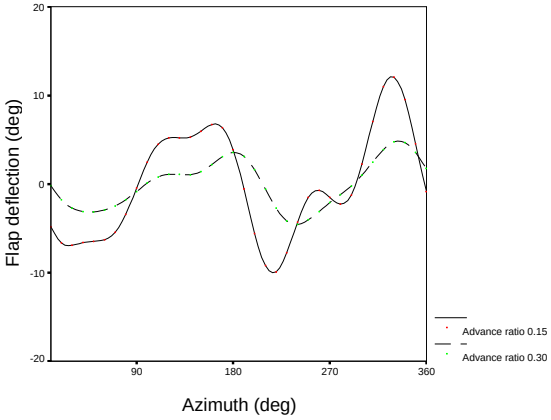

Figure 7. Flap deflection history at the advance ratios $\mu = 0.15$ and $\mu = 0.30$.

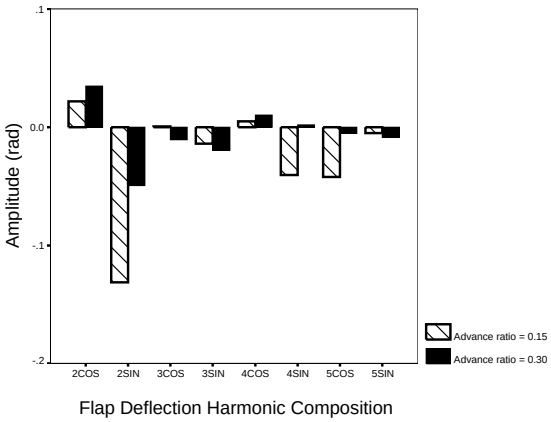

Figure 8. Flap deflection harmonic components at the advance ratios $\mu = 0.15$ and $\mu = 0.30$.

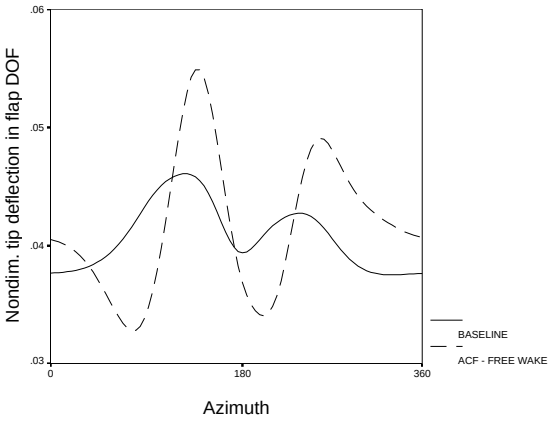

Figure 9. Nondimensional tip deflections in flap degree of freedom, $\mu = 0.15$.

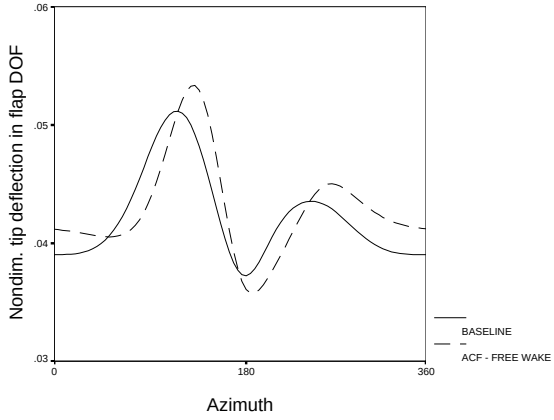

Figure 10. Nondimensional tip deflections in flap degree of freedom, $\mu = 0.30$.

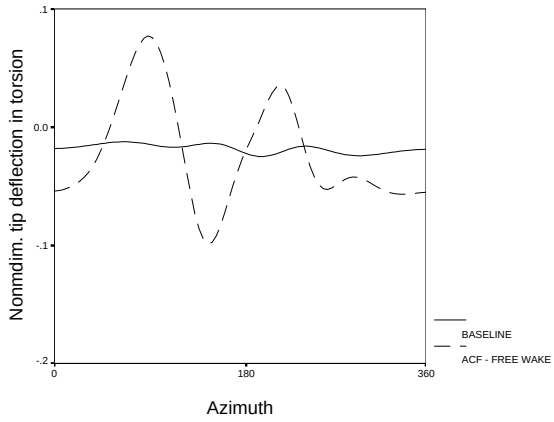

Figure 11. Nondimensional tip deflections in torsional degree of freedom, $\mu = 0.15$.

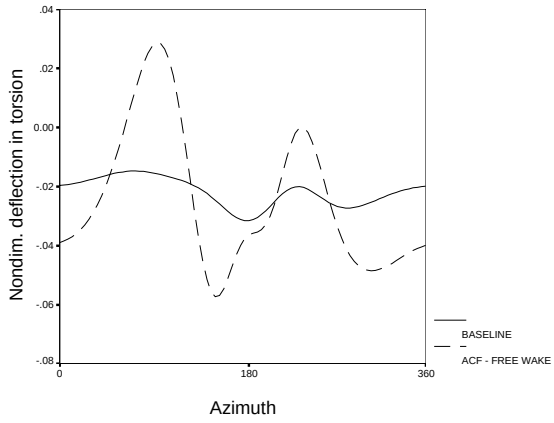

Figure 12. Nondimensional tip deflections in torsional degree of freedom, $\mu = 0.30$.

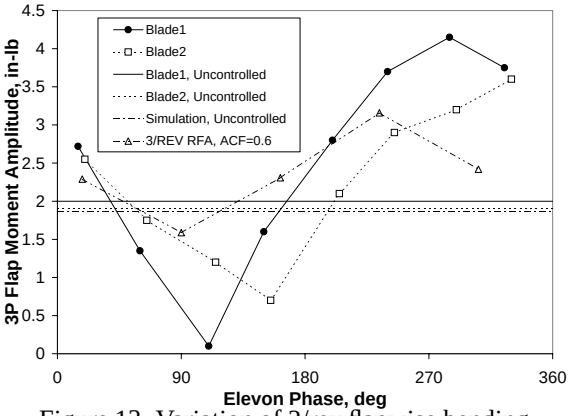

Figure 13. Variation of 2/rev flapwise bending moment with elevon phase, (760 RPM, $\mu = 0.20$, RFA aerodynamics).

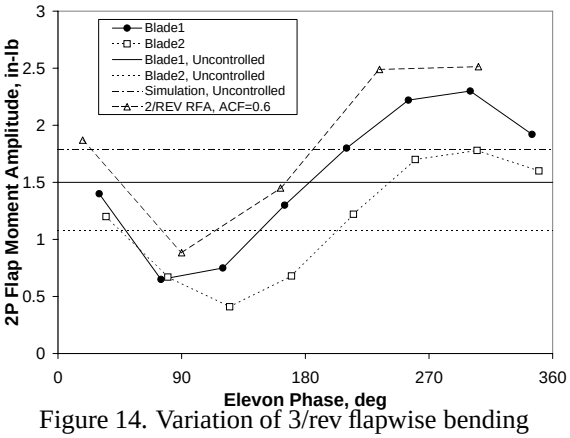

Figure 14. Variation of 3/rev flapwise bending moment with elevon phase, (760 RPM, $\mu = 0.20$, RFA aerodynamics).

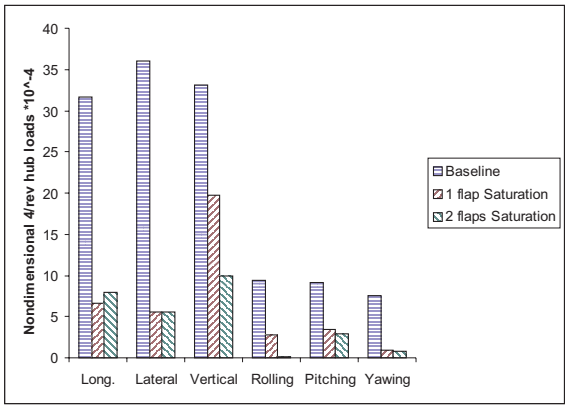

Figure 15. Vibration reduction with dynamic stall using single and dual flap configurations, with saturation limits, at $\mu = 0.35$).

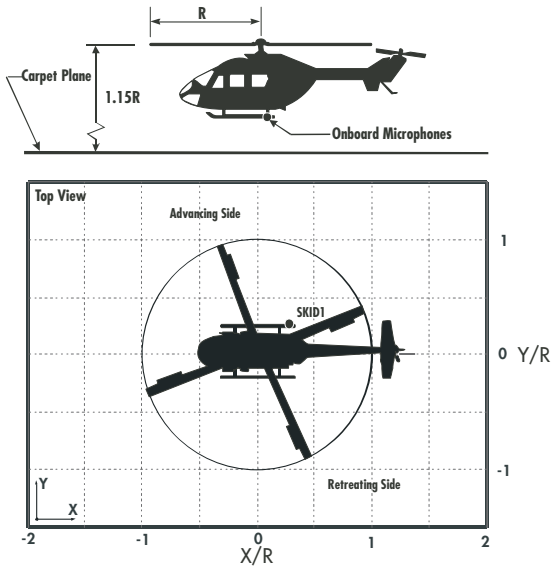

Figure 16: Microphone locations on and around the helicopter for noise feedback

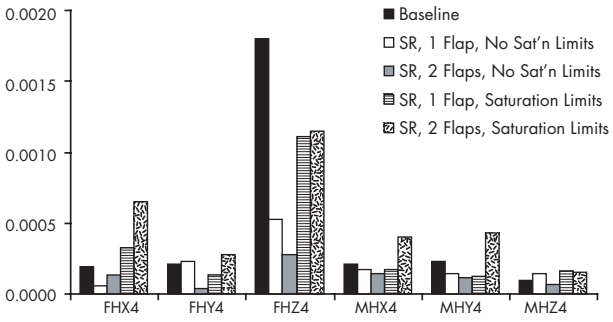

Figure 17: Vibration levels showing reduction from baseline, simultaneous reduction with 1 and 2 flaps

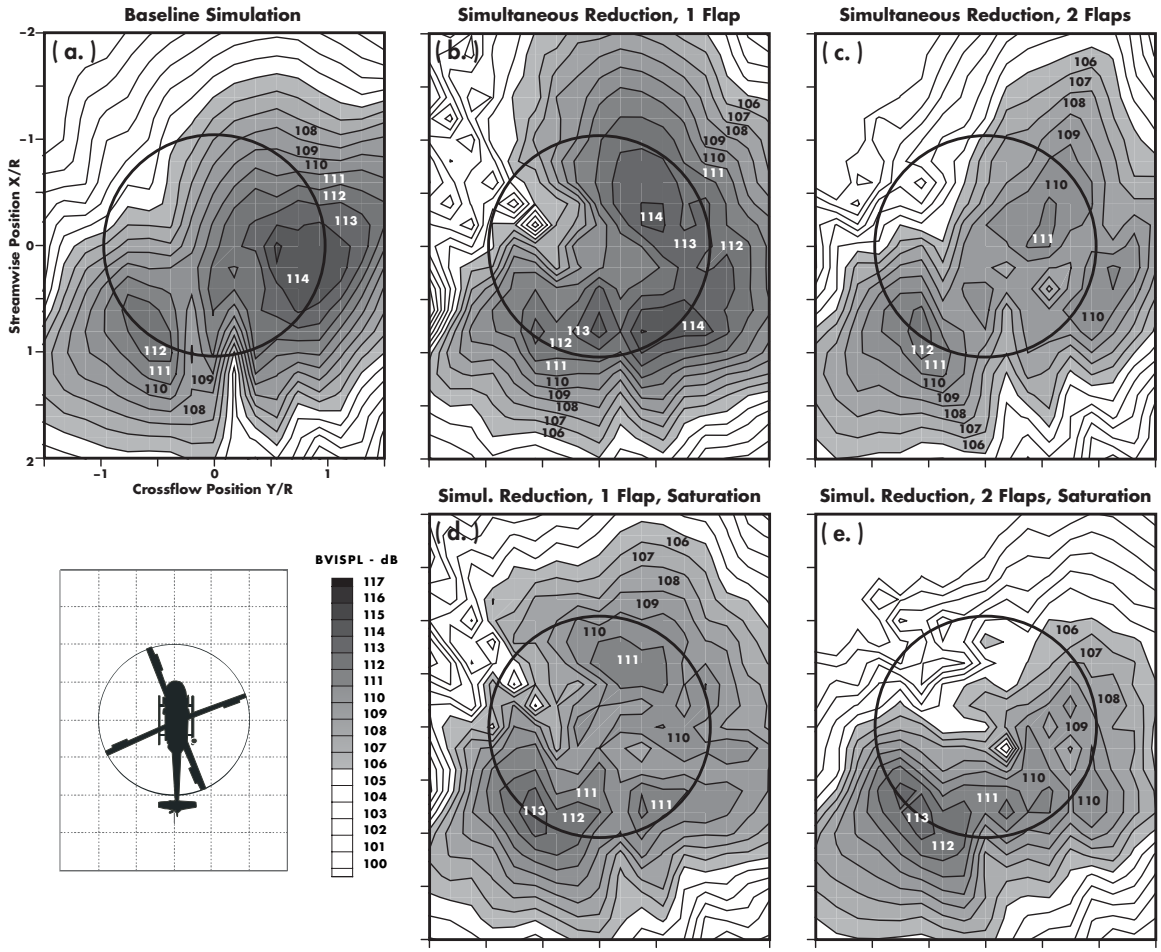

Figure 18: Noise carpet plot showing reduction from baseline, simultaneous reduction with 1 and 2 flaps